Excitation of dielectric barrier discharge using sinusoidal and nanosecond waveform: application to silicon solar cell

Rémy Bazinette, Jean Paillol, C. Laux, Delphine Bessières, F Massines

▶ **To cite this version:**

Rémy Bazinette, Jean Paillol, C. Laux, Delphine Bessières, F Massines. Excitation of dielectric barrier discharge using sinusoidal and nanosecond waveform: application to silicon solar cell. 22nd International Symposium on Plasma Chemistry, Jul 2015, Antwerp, Belgium. hal-01866309

HAL Id: hal-01866309
https://hal.science/hal-01866309

Submitted on 10 Sep 2018

HAL is a multi-disciplinary open access archive for the deposit and dissemination of scientific research documents, whether they are published or not. The documents may come from teaching and research institutions in France or abroad, or from public or private research centers.

L'archive ouverte pluridisciplinaire **HAL**, est destinée au dépôt et à la diffusion de documents scientifiques de niveau recherche, publiés ou non, émanant des établissements d'enseignement et de recherche français ou étrangers, des laboratoires publics ou privés.

Excitation of dielectric barrier discharge using sinusoidal and nanosecond waveform: application to silicon solar cell

R. Bazinette[1,2], J. Paillol[2], C.O. Laux[3], D. Bessière[2] and F. Massines[1]

[1] *Laboratoire PROcédés Matériaux et Energie Solaire, UPR 8521, Tecnosud, FR-66100 Perpignan, France*
[2] *SIAME, Université de Pau et des Pays de l'Adour, Pau, France*
[3] *Energétique Moléculaire et Macroscopique, Combustion (EM2C - Centrale Paris), Paris, France*

Abstract: Different diffuse dielectric barrier discharges (DBDs) are studied in the same configuration for different applied voltage waveforms: Glow, Townsend-like and radiofrequency (RF) DBD's for a sinusoidal excitation ranging from 50 kHz to 9 MHz and the nano-second repetitive pulsed DBD (NRP-DBD). The power of the RF and the NRP-DBD is 10 to 30 times larger than that of the low frequency DBD's but according to emission spectroscopy the electron energy and thus the energy transfer to the gas are quite different. The consequence on the chemical kinetic is illustrated by the difference in the conditions leading to a SiN:H having the same refractive index.

Keywords: DBD, homogeneous, glow, radiofrequency, nanopulse, silicon nitride

1. Introduction

Atmospheric pressure diffuse or homogeneous discharges are streamer free discharges. Low frequency diffuse dielectric barrier discharges (DBDs) have been abundantly studied [1]. Recently efforts have been made to increase the power of these discharges, in order to increase the efficiency of processes such as thin film growth. In the present work two solutions are compared: (i) the increase of the frequency excitation i.e., of the discharge repetition rate up to the point where the physics of the discharge change, adding wave riding to the ionization mechanisms, and (ii) the increase of the voltage up to a value largely higher than the breakdown voltage so rapidly that localized streamers are avoided thanks to a nanopulsed power supply. The aim of this work is to determine how the physics of homogeneous discharges change with the voltage waveform, and how this affects the induced chemistry through the analysis of thin film properties. The gas mixture is NH_3 diluted in Ar to have the benefit of NH_3 Penning ionization by Ar metastables to obtain a diffuse discharge when the excitation frequency and the voltage are low. SiH_4 is added to get SiNx:H thin films useful as antireflective and passivating thin films of p type silicon solar cells.

2. Experimantal set-up

Fig. 1 is a schematic view of the experimental reactor with two plasma areas defined by the two high-voltage electrodes metalized on an internal face of alumina square tubes. The ground electrode is on the other side of the 1 mm gap. It is also covered with an alumina plate. The metallization area is twice 14×50 mm^2 for high voltage (HV) electrodes and 50×50 mm^2 for the low-voltage one. A silicon wafer (CZ (100)) is used as a substrate to produce SiN coating at 400 °C. In this case, the substrate holder moves below the HV electrodes to cover the entire surface.

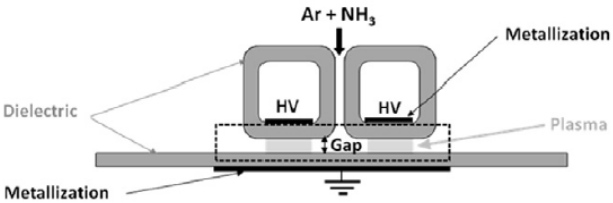

Fig. 1. Discharge cell.

The discharge cell is in an airtight reactor. The ambient air is removed with a primary vacuum, and the reactor is filled with argon up to a pressure of 760 Torr. The Ar flow rate is set to 3 l /min and the sum of NH_3 and SiH_4 is equal to 200 ppm. The waveforms used are: (i) a pulsed voltage generated by FID III (FPG20-30MkS50) generator to make pulses between 5 and 50 ns with a repetitive rate between 1 and 30 kHz. The high voltage electrode is always anode side. (ii) Sinusoidal voltage generated by waveform generator connected to an amplifier. Since the voltage at the output of the amplifier is not sufficient to ignite a discharge, the amplifier output is fed into a high-voltage transformer. Up to 60 kHz, an audio amplifier (Crest Audio CC4000) coupled to a high-voltage transformer with a large bandwidth is used. The maximum available voltage is 3 kV. The circuitry allows voltage and frequency to be independently adjusted. For higher frequency, we use the frequency resonance of the RLC circuit defined by the discharge cell capacitor and the inductance of a homemade transformer. The power injected is maximized and the power reflected is minimized. Different homemade transformers allow to work between 140 kHz and 9.6 MHz up to 1 kV. The amplifier is a PRANA GN500.

The discharge current is measured with a current probe (Lilco LTD 13W5000 400Hz-100MHz), and the voltage applied to the electrodes is measured with a high voltage probe (Tektronic P6015A 75 MHz). They are connected to a digital oscilloscope Tektronix DPO4104 (1 GHz). The average discharge power (P) is determined from the measurements of voltage (V(t)) and current (I(t)) over one cycle (T):

$$P = \frac{1}{T}\int_0^T V \cdot I \, \mathrm{d}t \qquad (1)$$

Plasma photographs are taken with an intensified CCD camera PI-MAX II (Princeton Instruments) with a camera lens working from 200 to 1100 nm. Exposure time can be as short as 5 ns.

Optical emission spectroscopy (OES) with long exposure time (100 ms) is made with a Maya2000Pro spectrometer which has a 14 µm square pixel size, slit of 25µm and an optic fiber of 600 µm with a collimator optic.

3. Results

3.1. Discharge modes

Fig. 2 presents the maximum value of the diffuse DBD power and the breakdown voltage as a function of the frequency between 1 kHz to 7.5 MHz for nanosecond repetitive pulsed and sinusoidal waveforms.

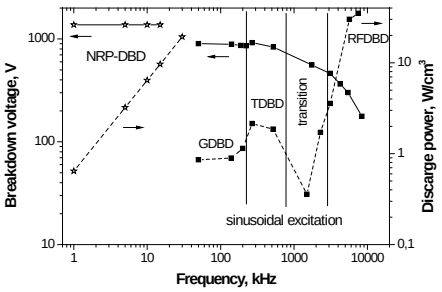

Fig. 2. Breakdown voltage (full line) and maximum power (dash line) of diffuse DBD as a function of voltage frequency for NRP and sinusoidal waveforms.

The FID generator works between 1 and 30 kHz. The pulse energy does not depend on the frequency and can reach 1.6 mJ for 50 ns. The power increases linearly with the repetitive frequency up to 25 W cm^{-3} but a filamentary discharge is observed above 17 W cm^{-3}. As the gas and the surface do not recover their initial properties however, the voltage increase is so high that the breakdown voltage is not affected. Its value is constant around 1.3 kV. Fast imaging shows that maximum plasma emission is close to the anode with weak emission close to the cathode (Fig. 3). This could be explained by emission from the cathode and the higher electron density close to the anode [2] associated to a rather uniform electric field.

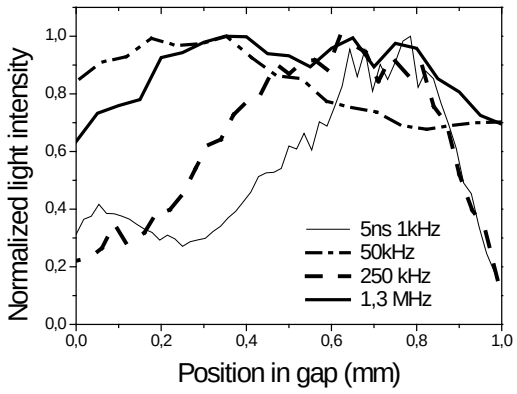

Fig. 3. Typical light profile from the anode (on the left) to the cathode (on the right) when the light is maximum for the different DBD modes.

For sinusoidal waveforms, the curves of Fig. 2 can be separated into four arrays corresponding to each discharge regime: glow, Townsend-like, transition and radiofrequency [**Error! Bookmark not defined.**]. At 50, 140 and 200 kHz the discharge operates in glow DBD (GDBD) mode characterized by a higher light emission close to the cathode (Fig. 3).

The power of this diffuse DBD is limited at around 1 W cm^{-3}. The breakdown voltage is almost constant at around 850 V because the lower excitation frequency (50 kHz) is high enough to enhance memory effects. Breakdown is controlled by ions drift (mainly NH_3^+), metastable diffusion and UV photons propagation inducing secondary emission from the cathode.

Between 270 and 520 kHz, the ion time transit from anode to cathode is longer than the voltage polarity inversion and according to the light intensity from the cathode to the anode, the cathode fall do not form (Fig. 3). In this range, the discharge is considered as a Townsend like DBD (TDBD) associated to a higher power because electrons have a larger energy than in the GDBD as the electric field is large whatever the position in the gap. The maximum power is twice that of a GDBD. It is associated with a decrease of the breakdown voltage due to ion accumulation in the gap which offers the possibility to drift to the cathode before breakdown-generating electrons. When the frequency further increases, ion trapping in the gap is more efficient. It enhances the positive space charge induced by electron displacement. The higher the frequency, the lower the breakdown voltage (150 V at 8.4 MHz). Around 1 MHz, there is a transition domain between TDBD and RFDBD where the power is lower than for other frequencies because the discharge is increasingly weakened by the gap.

Above 3 MHz, the amplitude of electron motion becomes smaller than the gap value limiting electron losses at the anode. Consequently, the discharge begins to be controlled by electron losses. The power density increases by a factor of 30 until 36 W cm^{-3}. This is not

the maximum value, as the voltage amplitude was limited by the power supply. In this range, the radiofrequency DBD (RFDBD) operates in alpha mode. The maximum ionization rate takes place in the plasma bulk at the sheath border due to sheath oscillation and in the bulk because of the rather high ion-electron recombination rate at atmospheric pressure.

As long as the discharge breakdown and development are controlled by the electron emission from the cathode, the power of the diffuse DBD is limited, but when the cathode does not largely participate in the ionization the power can be increased while still maintaining the diffuse mode.

The power increase induces a gas temperature increase (170 °C for 11 W cm^{-3}) i.e., a gas density decrease but this is not at the origin of the discharge stabilization. The temperature increase is much smaller in the case of NRP-DBD at least partly because of the small duty cycle. This is of interest to treat thermosensitive surfaces such as polymers.

3.2. Emission spectroscopy

The irradiance of G-, RF-, NRP-DBD is shown in Fig. 4. The main emissions lines depend on the discharge mode. We observe the$A^3\Pi–X^3\Sigma^-$ NH molecular band system at 330 and 336 nm and Ar* emission corresponding to transitions between different levels of $3p^54p$ (≈ 13 eV) and the four levels of $3p^54s$ (from 11.55 to 11.83 eV).

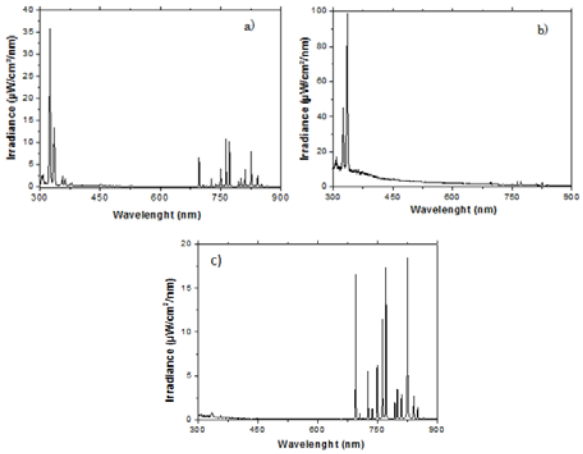

Fig. 4. Plasma irradiance: a) 50 kHz (GBDB), b) 9.6 MHz (RFDBD), and c) NRP-DBD (5 ns, 1 kHz).

In GDBD, NH emission at 342 nm dominates while at higher frequency (RFDBD) it is NH at 336nm and for the NRP-DBD it is Ar emissions. Ar emission is related to high energy electrons so the emission spectrum is a signature of electrons of higher energy than in the case of sinusoidal waveform.

For a sinusoidal voltage, the increase of the excitation frequency tends to decrease argon emission which is in agreement with a lower applied voltage and thus a lower electric field applied on the electrons. Moreover in RFDBD, a broad emission continuum in the UV/Vis range appears whereas argon emission is very weak. This continuum has been attributed to low energy electrons slowed down by the interaction with Ar atoms (Bremsstrahlung). This is observed in low pressure RF discharges [3] and is in agreement with the effect of the parameters: voltage and frequency increase the gas ionization and thus the electron density, N_e, whereas a temperature increase or pressure decrease reduces the density of Ar atoms, N_{gas}. At 9.6 MHz, the continuum is rather well fitted according to Eq. 2 assuming a Maxwellian distribution function, a mean electron energy of 1 eV and an electron density is between 10^{11} and 10^{12} per cm^3 because of a dual distribution function due to cold electrons is the bulk and high energy electrons coming from oscillations of the sheaths.

$$Q_\lambda d_\lambda = N_{gas} N_e h\nu \left(\int_{h\nu}^{\infty} \nu \frac{d\sigma_\nu(E)}{d\nu} \frac{d\nu}{d\lambda} f(E) dE \right) d\lambda \qquad (2)$$

$d\sigma(E)/d\nu$ is the Bremsstrahlung cross section calculated from e-Ar elastic cross-section modulated by photon emission.

The higher the continuum amplitude, the lower the argon emission and the higher the NH (336 nm) emission which is the one requiring the lowest electron energy. We conclude that, in RF-DBD, the electron energy is low compared to G-DBD and the density of electrons is higher. This is in agreement with the higher power and a lower breakdown voltage.

In conclusion, according to emission spectra and to the electrical behavior, the electron energy increases from RFDBD to GDBD and from GDBD to NRP-DBD.

3.3. Thin films

To illustrate the consequences of the DBD physics on chemical kinetics, the influence of the ratio $[NH_3]/[SiH_4]$ on SiN:H refractive index has been studied (Fig. 5). One advantage of SiN:H, is that its refractive index is easily tuned. Its value is directly correlated to the Si/N ratio in the film which is straightforwardly related to the ratio $R = [NH_3]/[SiH_4]$ [4]. Whatever the DBD mode, thin films made at 400 °C are dense, without porosity and it is always possible to optimize R to have coating properties compatible with the application. The optimum value for antireflective coating of crystalline silicon solar cells is 2.09 [5]. In GBDB, the optimum ratio is R = 1.75. In RFDBD, the NH_3 concentration must be increased and in NRP-DBD it has to be decreased.

This can be related to the difference in NH_3^+ flow to the surface. NH_3^+ is the dominant ion because Penning ionization is important, i.e., if the density of metastable integrated other time is high compared to that of electrons. And, moreover, charge transfer between Ar_2^+ and NH_3 is effective. In RFDBD, the density of metastable should be low, moreover ions are confined in the gas bulk and their contribution to the surface chemistry is low compared to the case of GDBD where they actively participate in the discharge development. The NRP-DBD is unipolar and the substrate was on the

cathode, so the flux of NH_3^+ should be rather high. This

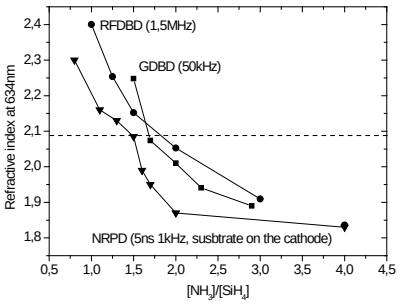

Fig. 5. Rrefractive index as a function of $[NH_3]/[SiH_4]$ for the different waveforms at 400 °C.

is confirmed by the increase of the refractive index, for the same NH_3/SiH_4 value, when the substrate is on the anode.

Fig. 6 presents the growth rate as a function of NH_3+SiH_4 obtained with the different DBD modes. For the GDBD, the growth rate saturates around 30 nm/min when the precursor concentration increases to 200 ppm. In that case, the growth rate is limited by the energetic species density, i.e., by the discharge power. The RFDBD which operated at higher power reaches 80 nm/min. The growth rate increases with precursor concentration showing that it is the precursor concentration that controls the growth rate. For the same power, similar growth rates are obtained with the NRP-DBD. If the power of that discharge is lower than that of GDBD, the growth rate is also lower. So we can conclude that more than the energy of electrons it is the power and the precursor concentration that control the growth rate.

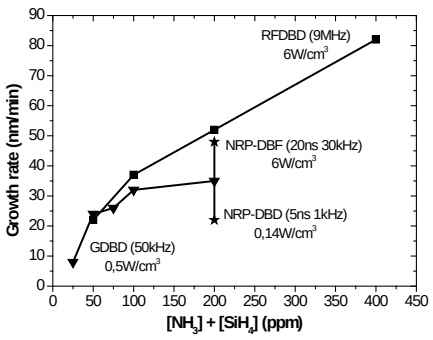

Fig. 6. Growth rate as a function of precursor concentration for the different waveforms.

4. Conclusions

The influence of the excitation waveforms on the behavior of a homogeneous DBD was studied. For sinusoidal excitation, three different discharge regimes are identified [6]. When the frequency increases, the discharge physics transitions from glow DBD to Townsend DBD and then to radiofrequency DBD. The transition from GDBD to TDBD is related to ion trapping in the gas gap. This is true until electrons begin to be trapped and ionization begins to be controlled by sheath oscillations. For GDBD in the 50 - 520 kHz range, the power varies markedly with the discharge regime: a factor of 2 was observed between GDBD and TDBD. The transition from TDBD to RFDBD is associated with a drastic increase of the power, related to higher electron density.

The RFDBD reaches 35 W cm^{-3} for the highest frequency tested. This large power increase is associated with a decrease in the breakdown voltage by a factor of 3, reflecting the variation of the dominant ionization mechanisms and electric field distribution over the gas gap. The electron density decreases between GDBD and TDBD, whereas the electron energy increases because of the field uniformity. In contrast, in the RFDBD the electron density is expected to be markedly higher, and with a lower electron energy associated with a Bremsstrahlung emission.

The NRP-DBD allows reaching much power than low frequency sinusoidal DBD with higher average electron energy. These different voltage waveforms allow to change the electron energy distribution function. Whatever the waveform, it is possible to obtain a dense layer of silicon nitride useful as antireflective coating for silicon solar cell but the optimized conditions depend on the plasma excitation. RFDBD and NRP-DBD allow to reach high growth rate.

4. Acknowledgements

It is a pleasure to acknowledge the "BATIR" FUI Project (F11211007U) financed by OSEO.

5. References

[1] F. Massines, N. Gherardi, N. Naude and P. Segur. *Eur. Phys. J. Appl. Phys.*, **47**, 22805 (2009)

[2] H. Takana and H. Nishiyama. in: *Proc. 21st Int. Symp. on Plasma Chemistry – ISPC 2013*. (Cairns, Australia) (2013)

[3] J. Park, I. Henins, H.W. Herrmann and G.S. Selwyn. *Phys. Plasmas*, **7**, 3141 (2000)

[4] P. Lecouvreur, *et al.* in: *Proc. 23rd Eur. Photovoltaic Solar Energy Conf.* 1581-1585 (2008)

[5] S. Quoizola, *et al.* in: *Proc. 25th Eur. Photovoltaic Solar Energy Conf.* 1800-1804 (2010)

[6] R. Bazinette, R. Subileau, J. Paillol and F. Massines. *Plasma Sources Sci. Technol.*, **23**, 035008 (2014)